Mapping inter-element coupling in metamaterials: Scaling down to infrared

E. Tatartschuk, N. Gneiding, F. Hesmer, A. Radkovskaya, and E. Shamonina

Citation: Journal of Applied Physics **111**, 094904 (2012); doi: 10.1063/1.4711092
View online: http://dx.doi.org/10.1063/1.4711092
View Table of Contents: http://scitation.aip.org/content/aip/journal/jap/111/9?ver=pdfcov
Published by the AIP Publishing

Mapping inter-element coupling in metamaterials: Scaling down to infrared

E. Tatartschuk,[1] N. Gneiding,[1] F. Hesmer,[2] A. Radkovskaya,[3] and E. Shamonina[4,a)]
[1]*Erlangen Graduate School in Advanced Optical Technologies, University of Erlangen-Nuremberg, 91052 Erlangen, Germany*
[2]*Department of Physics, University of Osnabrück, 49069 Osnabrück, Germany*
[3]*Magnetism Division, Faculty of Physics, M. V. Lomonosov Moscow State University, Leninskie Gory, Moscow 119992, Russia*
[4]*Optical and Semiconductor Devices Group, Electrical and Electronic Engineering (EEE) Department, Imperial College, Exhibition Road, London SW7 2BT, United Kingdom*

(Received 29 September 2011; accepted 9 April 2012; published online 7 May 2012)

The coupling between arbitrarily positioned and oriented split ring resonators is investigated up to THz frequencies. Two different analytical approaches are used, one based on circuits and the other on field quantities that includes retardation. These are supplemented by numerical simulations and experiments in the GHz range, and by simulations in the THz range. The field approach makes it possible to determine separately the electric and magnetic coupling coefficients which, depending on orientation, may reinforce or may cancel each other. Maps of coupling are produced for arbitrary orientations of two co-planar split rings resonant at around 2 GHz and then with the geometry scaled down to be resonant at around 100 THz. We prove that the inertia of electrons at high frequencies results in a dramatic change in the maps of coupling, due to reduction of the magnetic contribution. Our approach could facilitate the design of metamaterials in a wide frequency range up to the saturation of the resonant frequency. © *2012 American Institute of Physics*.
[http://dx.doi.org/10.1063/1.4711092]

I. INTRODUCTION

Metamaterials are artificially created structures with unusual electric and magnetic properties that are difficult or impossible to find in nature. The initial upsurge of interest was triggered by verifications of new phenomena which come about when negative permeability and negative permittivity can be simultaneously realized in the same frequency band,[1–3] including the concept of the perfect lens.[4] New potential applications (e.g., invisibility cloaks) have been emerging at a high rate, and considerable progress has been made on both the theoretical[5] and experimental[6,7] fronts.

The building blocks of metamaterials are resonant elements much smaller than the wavelength of the electromagnetic wave which can be seen as "artificial atoms" with strong electric and/or magnetic response to the electromagnetic radiation. The main advantage of metamaterials over naturally occurring materials is that their electromagnetic properties can be designed and controlled by choosing the shape of the elements and the way they are arranged within the structure.[8–10] However, not only the resonant properties of single elements[11,12] influence the electromagnetic response of a metamaterial structure but also coupling between the resonators can change the effective parameters, inducing a strong spatial dispersion.[13,14] Another effect is that inter-element coupling gives rise to slow waves. They have been introduced in 2002 under the name of magnetoinductive waves,[15,16] pointing out the magnetic nature of the capacitively loaded loops interaction.[17] Magnetoinductive waves are also known as magnetic plasmons[18–20] and magnetization waves.[21] If the interaction between the resonators appears to have electric character, the corresponding term is electroinductive wave.[22,23] Depending on the sign of the coupling coefficient, these waves can have positive or negative group velocity.[24] Coupling effects have potential in applications such as magnetoinductive lens,[25–28] amplifiers for MRI,[29] polarizers,[30] etc. Obviously, to be able to effectively employ metamaterials for the manipulation of the electromagnetic fields, it is crucial to understand their "microscopic" properties, i.e., the way how the electric and magnetic fields are created and the details of the coupling mechanism between the elements. A microscopic investigation of this kind has been recently undertaken by Powell *et al.*[31] using singly split rings as the resonant elements. They employed the axial configuration with two elements and investigated the effect of the rotation of one element relative to the other on the strength and sign of coupling.

In this paper, we employ a method of calculating inter-element coupling coefficients for arbitrarily assembled 3D split-ring metamaterials to account for the major scenarios occurring in a range from GHz to near infrared. By separately evaluating electric and magnetic contributions to the coupling coefficient, we are able to map the inter-element coupling for arbitrary positions and orientations of the elements. The paper is organized as follows. We present an analytical model for working out the coupling between arbitrarily positioned and oriented split rings in Sec. II, using both a circuit and a field approach. In Sec. III, a variety of configurations is systematically analyzed in the GHz and THz frequency regimes. Conclusions are drawn in Sec. IV.

a)e.shamonina@imperial.ac.uk.

II. COUPLED RESONATORS: THEORY

A. Circuit approach

The elements studied in this paper are singly split metal rings as shown in Fig. 1(a), where R is the inner radius, w is the wall thickness, h is the wall height, and g is the gap width. They can be modeled by equivalent LCR circuits (Fig. 1(b)). Our main interest is to find out how two such rings are coupled to each other for arbitrary orientations and assess the relative significance of magnetic and electric couplings. Our element, as may be expected, will exhibit a single resonance. When two such elements are brought close to each other, the coupling between them manifests itself in a split of the resonance, a well known phenomenon. Assuming two arbitrarily positioned elements, there can be both electric and magnetic coupling, and, if the rings are in direct contact, conductive coupling is present as well.[32] The magnetic and electric coupling coefficients for two identical split rings can be defined with the aid of the coupled LCR circuits shown in Fig. 1(c) as

$$\kappa_H = \frac{2M}{L}, \quad \kappa_E = \frac{2C}{K}, \tag{1}$$

where L and C are the self-inductance and self-capacitance and M and K are the mutual inductance and the mutual capacitance, respectively. In general, depending on the relative position and orientation of two such elements, and on their individual properties, either of the coupling coefficients may become dominant. Note also that both coupling coefficients may be complex quantities due to retardation.

The theoretical approach can start with a Lagrangian for two coupled split rings that can be written as

$$\mathcal{L} = \frac{L(\dot{q_1}^2 + \dot{q_2}^2)}{2} - \frac{q_1^2 + q_2^2}{2C} + M\dot{q}_1\dot{q}_2 - \frac{q_1 q_2}{K}, \tag{2}$$

where q_l is the charge on the capacitor in element l ($l = 1, 2$) and the dot denotes the time derivative. Next, we

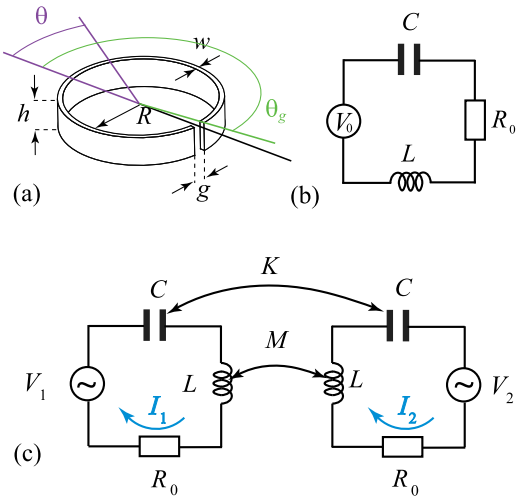

FIG. 1. Singly split metal ring resonator (a) and its equivalent circuit (b). Equivalent circuit for two coupled rings. Both electric (K) and magnetic (M) couplings are assumed (c).

use the Euler equation for driven dissipative systems (see, e.g., Ref. 18)

$$\frac{d}{dt}\left(\frac{\partial \mathcal{L}}{\partial \dot{q}_l}\right) - \frac{\partial \mathcal{L}}{\partial q_l} = V_l - R_0\dot{q}_l, \tag{3}$$

where the expression on the right hand side represents generalized forces for element l due to the driving voltage V_l and the dissipation of energy due to losses (term with the resistance R_0). Using Eq. (3), we may convert Eq. (2) into a set of two differential equations in terms of the currents, $I_l = \dot{q}_l$. For harmonic time variation in the form $\exp(-i\omega t)$, we can perform the operations in Eq. (3) to arrive at Kirchhoff's voltage equations

$$\begin{aligned} Z_0 I_1 - i\omega\, MI_2 - \frac{1}{i\omega K} I_2 &= V_1, \\ Z_0 I_2 - i\omega\, MI_1 - \frac{1}{i\omega K} I_1 &= V_2, \end{aligned} \tag{4}$$

where

$$Z_0 = R_0 - i\omega L - \frac{1}{i\omega C} = -i\omega L\left(\frac{i}{Q'} + 1 - \frac{\omega_0^2}{\omega^2}\right) \tag{5}$$

is the self-impedance, $\omega_0 = 1/\sqrt{LC}$ is the resonant frequency, and

$$Q' = Q\frac{\omega}{\omega_0}, \quad \text{with} \quad Q = \frac{\omega_0 L}{R_0} \tag{6}$$

being the quality factor. Assuming asymmetric excitation with only element 1 driven ($V_1 = V_0$, $V_2 = 0$), we obtain for the frequency dependence of the currents

$$\begin{aligned} I_1 &= -\frac{iV_0}{D}\left(\omega L - \frac{1}{\omega C} + \frac{i}{Q'}\right), \\ I_2 &= -\frac{iV_0}{D}\left(\omega M - \frac{1}{\omega K}\right), \end{aligned} \tag{7}$$

with

$$D = \left(\omega L - \frac{1}{\omega C} + \frac{i}{Q'}\right)^2 - \left(\omega M - \frac{1}{\omega K}\right)^2. \tag{8}$$

By measuring, or obtaining from simulation, the ratio I_2/I_1 as a function of frequency, the total coupling coefficient, $\kappa_{\text{total}} = \kappa_H - \kappa_E$, can be determined

$$-2\frac{I_2}{I_1}\left(1 - \frac{\omega_0^2}{\omega^2} + \frac{i}{Q'}\right) = \kappa_H - \kappa_E\frac{\omega_0^2}{\omega^2} \approx \kappa_H - \kappa_E \tag{9}$$

but not the contributions of magnetic and electric coupling separately.

B. Field approach

Our intention here is to determine the coupling coefficient with the aid of the charge and current densities in the split rings. We can start with some well known relationship[33]

between magnetic energy, W_m, current, $\vec{J}$, and vector potential, $\vec{A}$, in the form

$$W_m = \frac{1}{2}\int \vec{A}\cdot\vec{J}d\tau, \tag{10}$$

where $d\tau$ is a volume element. The expression for the vector potential in terms of current densities is also well known. When retardation is included, the vector potential can be expressed in terms of the current that creates it as

$$\vec{A}(\vec{r}) = \frac{\mu_0}{4\pi}\int \frac{\vec{J}(\vec{r'})e^{ik|\vec{r}-\vec{r'}|}}{|\vec{r}-\vec{r'}|}d\tau', \tag{11}$$

where μ_0 is the free-space permeability, k is the free-space wave number, $\vec{r}$ and $\vec{r'}$ are position vectors of the vector potential and of the current density, respectively. We may now substitute Eq. (11) into Eq. (10) to obtain the full expression for the magnetic energy. But, before we do so, we note that our interest is restricted to the mutual magnetic energy that can then be written as

$$W_{m,mut} = \frac{1}{2}\int(\vec{A_1}\cdot\vec{J_2} + \vec{A_2}\cdot\vec{J_1})d\tau, \tag{12}$$

where $\vec{J_1}$ and $\vec{J_2}$ are the current densities in rings 1 and 2, $\vec{A_1}$ is the vector potential created by current in ring 1, and $\vec{A_2}$ is the vector potential created by the current in ring 2. Due to symmetry, $\int \vec{A_1}\cdot\vec{J_2}d\tau = \int \vec{A_2}\cdot\vec{J_1}d\tau$ hence the mutual magnetic energy can be expressed as a double integral

$$W_{m,mut} = \frac{\mu_0}{4\pi}\int\int \frac{\vec{J_1}(\vec{r}_1)\cdot\vec{J_2}(\vec{r}_2)e^{ik|\vec{r}_1-\vec{r}_2|}}{|\vec{r}_1-\vec{r}_2|}d\tau_1 d\tau_2, \tag{13}$$

with integration over volumes of both rings only. Here, $d\tau_l$ is the volume element of ring l and $\vec{r}_l$ is its position vector. Note that a simplified version of this expression, disregarding the retardation term $e^{ik|\vec{r}_1-\vec{r}_2|}$, has been widely used (see, e.g., Refs. 33 and 34).

Next, we introduce the often used approximation that the current density is to be replaced by a filament current, $\vec{I}$, i.e., we ignore the variation of the current density across the cross section. Then, Eq. (13) takes the form

$$W_{m,mut} = \frac{\mu_0}{4\pi}\int\int \frac{\vec{I_1}(\vec{r}_1)\cdot\vec{I_2}(\vec{r}_2)e^{ik|\vec{r}_1-\vec{r}_2|}}{|\vec{r}_1-\vec{r}_2|}ds_1 ds_2, \tag{14}$$

where ds_l is the line element along the filament (see Fig. 2(a)). Let us recall that the mutual inductance is defined as

$$W_{m,mut} = MI_1I_2, \tag{15}$$

where, of course, the total currents I_1 and I_2 (that includes the displacement current as well) are independent of space. Considering that the total current is conserved along the perimeter of the ring, our final expression for the mutual inductance M takes the form

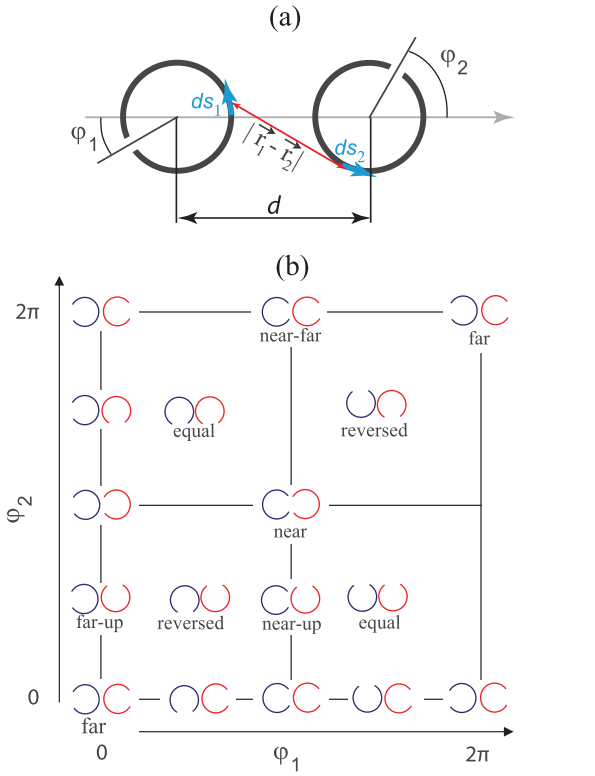

FIG. 2. Top view of the pair of arbitrarily oriented split rings in the planar configuration (a). Configurations in the $\varphi_1 - \varphi_2$ plane showing schematically the positions "near," "far," "equal," "reversed," "near-far," "near-up," and "far-up" (b).

$$M = \frac{\mu_0}{4\pi}\int\int \frac{\vec{I}_{n1}(\vec{r}_1)\cdot\vec{I}_{n2}(\vec{r}_2)e^{ik|\vec{r}_1-\vec{r}_2|}}{|\vec{r}_1-\vec{r}_2|}ds_1 ds_2, \tag{16}$$

where $\vec{I}_{nl}$ are now dimensionless quantities reaching their maximum value of unity for the angular coordinate $\theta = 0$ (see Fig. 1(a)).

The mutual electric energy may be obtained by an analogous derivation in which the scalar potential and the charge density are used. It comes to a similar double integral

$$W_{e,mut} = \frac{1}{4\pi\varepsilon_0}\int\int \frac{\rho_1(\vec{r}_1)\rho_2(\vec{r}_2)e^{ik|\vec{r}_1-\vec{r}_2|}}{|\vec{r}_1-\vec{r}_2|}d\tau_1 d\tau_2, \tag{17}$$

where ε_0 is the free-space permittivity. Note that a simplified version of this expression, disregarding the retardation term $e^{ik|\vec{r}_1-\vec{r}_2|}$, has been widely used (see, e.g., Refs. 33 and 34).

In terms of circuit quantities

$$W_{e,mut} = \frac{1}{K}Q_1Q_2, \tag{18}$$

where $Q_l = Q_c$ is the total charge on one half (between the gap and the half-point where the charge is zero) of ring l. Changing now to line charge and taking the integration over the perimeter of the ring, the mutual capacitance may be obtained as

$$K^{-1} = \frac{1}{4\pi\varepsilon_0}\int\int \frac{\rho_{Ln1}(\vec{r}_1)\rho_{Ln2}(\vec{r}_2)e^{ik|\vec{r}_1-\vec{r}_2|}}{|\vec{r}_1-\vec{r}_2|}ds_1 ds_2, \tag{19}$$

where $\rho_{Ln/}$ are the normalized line charges. For evaluating the integrals, we need functional relationships for the filament currents and for the charge distribution. For finding the coupling coefficients, we need the self-capacitance and self-inductance of the rings and also the expression for the charge. These can be calculated analytically on the basis of the paper by Allen and Segre[35] who found analytically the electric field distribution in an infinitely thin split metallic cylinder. The expressions derived were extended by Sydoruk *et al.*[11] for a ring of finite size. Further generalizations were affected by Delgado *et al.*[36] by including kinetic inductance.

The charge distribution in the split ring is given as

$$\rho_L(\theta) = \frac{h+w}{\pi}\varepsilon_0 V_0 \tan\frac{\theta}{2} \quad \text{for} \quad \theta \le \theta_g, \tag{20}$$

where $\pm\theta_g$ are the coordinates of the gap (see Fig. 1(a)). Integrating Eq. (20) over θ from 0 to θ_g will give the total charge Q_c in the form

$$Q_c = 2R\frac{h+w}{\pi}\varepsilon_0\, V_0 \ln\left(\sin\frac{g}{4R}\right). \tag{21}$$

With the aid of the continuity equation, we find the current as

$$I(\theta) = -i\omega 2R\frac{h+w}{\pi}\varepsilon_0\, V_0 \ln\left(\frac{\cos\frac{\theta_g}{2}}{\cos\frac{\theta}{2}}\right), \tag{22}$$

satisfying the boundary condition that the current vanishes at the gap, i.e., $I(\pm\theta_g) = 0$, and, of course, there is no conduction current in the gap. The maximum of Eq. (22) occurs at $\theta = 0$. Hence, the normalized current is of the form

$$I_n(\theta) = \ln\left(\frac{\cos\frac{\theta_g}{2}}{\cos\frac{\theta}{2}}\right)\ln^{-1}\left(\cos\frac{\theta_g}{2}\right). \tag{23}$$

The approximate values of the self-inductance and self-capacitance are

$$L = \mu_0 R\left(\ln\frac{8R}{h+w} - \frac{1}{2}\right) \tag{24}$$

and

$$C = \varepsilon_0\left[\frac{(w+g)(h+g)}{g} + \frac{2(h+w)}{\pi}\ln\frac{4R}{g}\right]. \tag{25}$$

We wish to emphasize the advantage of the field method over the circuit method: we are able to separately determine the magnetic and electric contributions to the total coupling coefficient, gaining an insight into the relative importance of the two coupling mechanisms.

III. ORIENTATIONAL MAPS

A. Microwave regime

We are now in a position to determine analytically all three coupling coefficients of interest: the electric, the magnetic, and the total coupling coefficient. We take as an example two arbitrarily oriented co-planar split rings of inner radius, $R = 10$ mm, wall thickness, $w = 0.1R$, wall height, $h = 0.5\,R$, and gap width of $g = 0.15\,R$ at a distance $d = 24$ mm between the centers of the rings. The orientation of the rings is specified by the coordinates φ_1 and φ_2 as shown in Fig. 2(a). Some of the configurations for certain discrete values of φ_1 and φ_2 are displayed in Fig. 2(b). For example, the "near" configuration, when the gaps are near to each other, has the coordinates $\varphi_1 = \varphi_2 = \pi$.

The amplitude and phase of the analytically obtained coupling coefficients (total, electric, magnetic) are shown in Fig. 3. As expected, the maximum overall coupling occurs in the "near" case. It may also be seen that, depending on the relative orientation, the total coupling may be dominated either by its electric part (e.g., in the configuration "near") or by its magnetic part (e.g., in the configuration "far"), as can be conveniently deduced from the maps for κ_H and $-\kappa_E$. The coupling coefficients in Fig. 3 are bound to be complex due to retardation. In contrast when retardation is disregarded, all the coupling coefficients must be real, positive, or negative. The corresponding orientational maps are shown in Fig. 4. As expected, the maximum negative coupling is observed for the configuration "far." Some of the results are though unexpected. In spite of the rings being in the planar configuration, the magnetic coupling is not everywhere

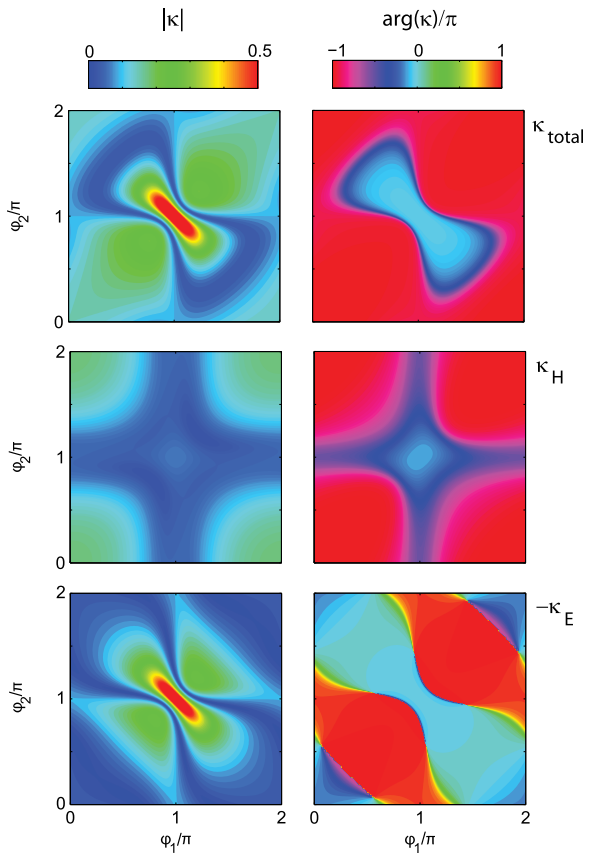

FIG. 3. GHz regime. Analytically calculated orientational maps including retardation ($R = 10$ mm, $d = 24$ mm, and $f_0 = 1.874$ GHz) showing the total coupling coefficient ($\kappa_{total} = \kappa_H - \kappa_E$, top), and its magnetic (κ_H, 2nd row) and electric ($-\kappa_E$, bottom) contributions for the configurations of Fig. 2. Left: amplitude; right: phase of the coupling coefficient.

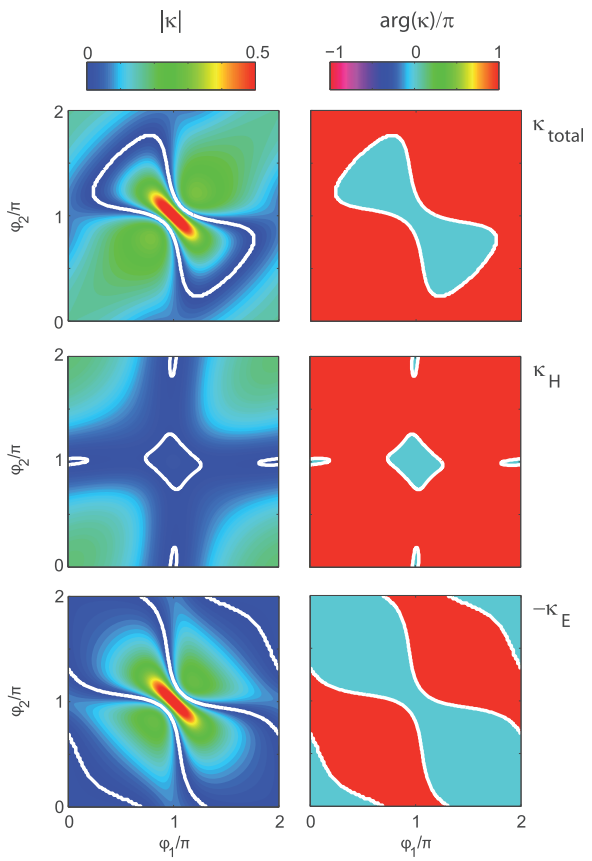

FIG. 4. Effect of retardation. Analytically calculated orientational maps of the coupling coefficient for the same parameters as in Fig. 3 except with retardation being switched off.

negative. For example, in the configuration "near" the magnetic coupling is positive although weak. This can be explained from the magnetic field distribution created by a single ring. In the case of a closed metallic coil, the induced magnetic field just outside the ring would always be opposed to the field just inside the ring: this would result in a negative magnetic coupling coefficient if another ring were placed just outside. However, due to the gap in the ring, the magnetic field may "leak" outside[37] and the coupling may become positive. It follows then that for a slightly tilted configuration, the magnetic coupling will be zero and this is indeed borne out by the maps of Fig. 4.

Next, let us look at the electric coupling without retardation (Fig. 4, 3rd row). As expected, the strongest positive coupling is for the configuration "near." In the configuration "far" and "equal," the coupling is positive, but in the configuration "reverse," it is negative. Thus, in the configuration "near," the magnetic and electric coupling, both being positive, reinforce each other, whereas in the configuration "reversed," both terms are negative, again, reinforcing each other. In the configurations "far" and "equal," the coupling is dominated by the magnetic interaction, but the electric interaction acts in the opposite direction thus reducing the total coupling. An interesting situation occurs for two configurations with the gaps oriented perpendicular to each other, "near-up" and "far-up," employed in Refs. 38 and 39 in constructing a metamaterial polarizing sheet. As can be seen from Fig. 4 in the "far-up" configuration, the coupling is mostly magnetic and negative; whereas in the "near-up" configuration, it is mostly electric and negative.

Retardation does not change dramatically this picture (cf. Figs. 3 and 4), but its effect is more pronounced for orientations with weak coupling. The configurations "near" and "far" are the ones least affected by retardation. This makes good sense: close proximity of the dominant charges (or currents) has two consequences: strong electric (or magnetic) coupling coefficient but also small retardation effect. The effect of retardation is however quite strong (phase change in κ_{total} more than $\pi/5$ relative to the case without retardation) in those cases, where κ_H and $-\kappa_E$ are either both too weak (e.g., configurations "near-up" and "near-far") or where the two contributions have opposite signs and nearly cancel each other (e.g., configuration "equal").

We have also determined the total coupling coefficient from CST simulations[40] for 21×21 different $\varphi_1 \times \varphi_2$ combinations. Two split rings were simulated at a frequency of $f = 1.874$ GHz assuming a quality factor of 27.6. One of the rings was excited by a current source in the gap. The resultant currents were obtained by probes monitoring the magnetic fields in the centres of the elements. We need to emphasize here that determining the currents is not sufficient for finding separately the electric and magnetic coupling coefficients. On the other hand, we are able to find the total coupling coefficient by substituting the values of the currents into Eq. (9). It may be seen in Fig. 5 that all the main features of the analytical solution are reproduced by the numerical one. We need to emphasize that this is genuine agreement; there is not a single free fitting parameter in the procedure. The only difference between the analytical and numerical data is a slight asymmetry of the latter relative to the diagonal axis seen in Fig. 5. This is due to the asymmetry of the excitation—independently of the relative position of the two split rings, the left one was always excited.

We have done so far the calculations for one separation of $d = 24$ mm between the elements. Obviously, the coupling is bound to decline as the separation increases. One would expect that other features, e.g., the dependence of coupling on the orientation of the elements will not be strongly affected. This is borne out by the plots shown in Fig. 6 for $d = 34$ mm (cf. Fig. 3). Here, however, a better agreement between the analytical calculations and the simulated/

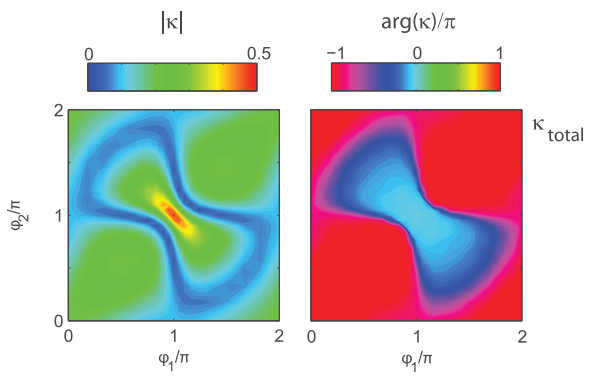

FIG. 5. Numerically calculated orientational maps of the total coupling in the GHz regime for the same parameters as in Fig. 3.

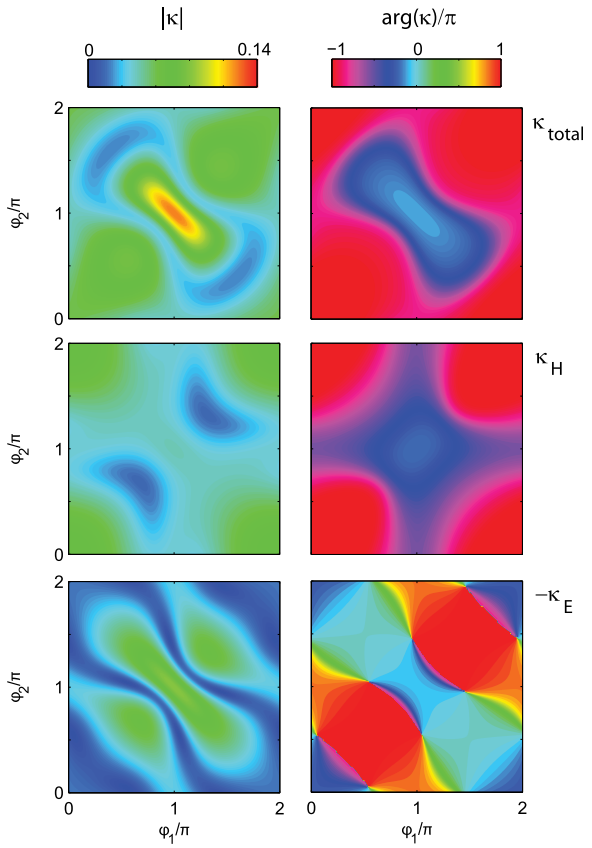

FIG. 6. Effect of separation. Analytically calculated orientational maps for the same parameters as in Fig. 3 except for $d = 34$ mm.

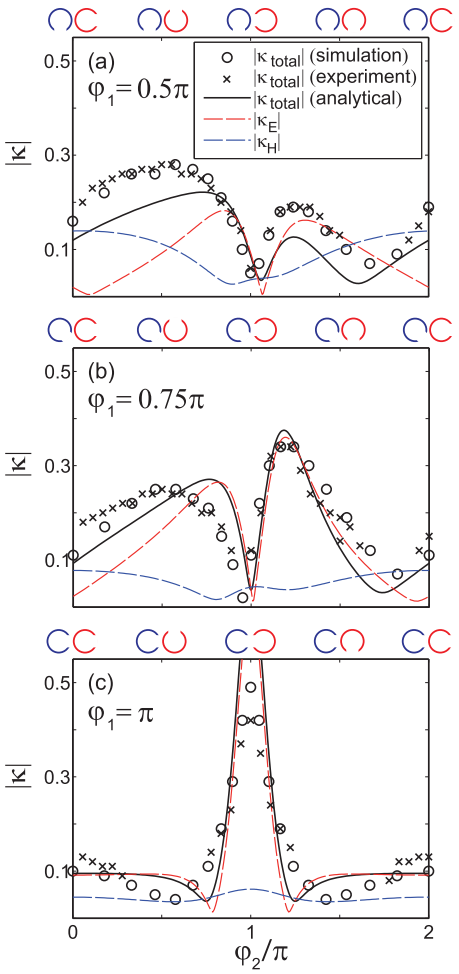

FIG. 7. GHz regime ($R = 10$ mm, $d = 24$ mm, and $f_0 = 1.874$ GHz). Measured, simulated, and analytically calculated coupling coefficients vs. φ_2 for $\varphi_1 = 0.5\pi$ (a), 0.75π (b), and π (c).

experimental results may be expected: the larger the separation, the more valid the filament model.

Further studies of the effect of separation have shown little of interest, but one point is worth mentioning namely the effect upon the "near" configuration. We know that the dominant contribution there is from the electric coupling, but this coupling happens to decline with distance faster than the magnetic one so that at a distance twice the element diameter both contributions become equally important. Being practically in phase, the magnetic and electric coupling reinforce each other acquiring an additional phase due to the retardation as the distance increases.

We have also performed a series of measurements on two coupled split rings of the same geometry as in the numerical simulations and retrieved the coupling coefficient from the circuit model discussed in Sec. III A. The setups used in experiment consist of a transmitter antenna exciting one of the two identical rings lying in the same plane and a receiving antenna detecting the field under the rings. A detailed description of the setup can be found in Ref. 37. Thus, at that particular frequency range, we have, in addition to analytical and numerical data, experimental data as well. Note that from experiments, as well as from numerical simulation data, only the total coupling coefficient can be calculated with the aid of the circuit model.

Comparisons between the various methods are shown in Fig. 7 where the amplitudes of the coupling coefficients are plotted as functions of φ_2/π for three different values of $\varphi_1 = \pi/2$, $3\pi/4$, and π in subplots of (a), (b), and (c), respectively. The electric and magnetic coupling coefficients calculated analytically are shown by thin dotted lines in red and blue, respectively. The experimental points are denoted by crosses, the simulated ones by small circles, and the analytical results for the total coupling coefficient by a thick black line. The crosses, circles, and the thick black line are in excellent agreement. The agreement with the analytical results is good in Figs. 7(a) and 7(b) although somewhat worse in Fig. 7(c). In particular for the "near" configuration, the total coupling coefficient is considerably higher from the analytical expression than from simulation. The likely reason is that this is the case when the strongest interaction occurs so the approximations introduced in calculating the current and charge distributions in the individual elements are less valid. We may however claim in general that our analytical model is capable of predicting the coupling strength and separate the electric and magnetic contributions. All salient features of the coupling are well reproduced.

B. THz regime

It has been shown experimentally some time ago that split rings as metamaterial elements are still effective at THz

frequencies.[41] It was shown by Zhou *et al.*[42], Klein *et al.*,[43] and Tretyakov[44] that as the size of the elements declines the frequency increases until saturation eventually sets in. The reason is the inertia of the electrons flowing in a metal structure. Inertia of the electrons means that the current appears only after a certain delay following excitation, the effect similar to that produced by a magnetic field. Hence, the effect can be simply accounted for by an additional inductance, the so-called kinetic inductance (see, e.g., Ref. 45), which within the Drude model can for the split ring be approximated by

$$L_{\text{kin}} = \frac{2\pi R}{wh\omega_{\text{p}}^2\varepsilon_0}, \tag{26}$$

where ω_{p} is the plasma frequency, so that the expression for the resonant frequency takes the form

$$f_0 = \frac{1}{2\pi\sqrt{(L_{\text{mag}} + L_{\text{kin}})C}}. \tag{27}$$

Our intention in this section is to demonstrate that at high frequencies not only the resonant frequency but also the inter-element coupling undergoes dramatic changes as the kinetic inductance becomes significant due to the small dimensions.

Are there additional considerations as the frequency increases that need to be taken into account apart from the inertia of the electrons? One consequence of the saturation of the resonance due to the electron's inertia is a reduction of the effect of radiative losses as element's dimensions become smaller relative to the wavelength. On the other hand, an opposite effect that arises when scaling down the dimensions at higher frequencies is a dramatic increase of loss due to boundary scattering which becomes important when the electrons' mean free path exceeds the size of the element (see, e.g., Refs. 46 and 47). In addition, the effect of reduced size is that the boundaries can no longer be regarded as planes: surface roughness must be taken into account.[47] Both effects due to boundary scattering could be incorporated into the model by including an additional resistance. However, this additional loss will not affect our conclusions regarding coupling between the elements and we disregard it here in order not to obscure the main argument. We shall now concentrate upon the effect of kinetic inductance because that is the major factor: it is the one that makes the THz regime different from the GHz regime.

At GHz frequencies, we were entitled to use for self-inductance in Eq. (1) only the magnetic inductance obtained, e.g., analytically from Eq. (24)

$$\kappa_H = \frac{2M}{L} = \frac{2M}{L_{\text{mag}}}(\text{GHz}). \tag{28}$$

At THz frequencies, we have to include into the expression for the self-inductance the kinetic inductance from Eq. (26) as well

$$\kappa_H = \frac{2M}{L} = \frac{2M}{L_{\text{mag}} + L_{\text{kin}}}(\text{THz}). \tag{29}$$

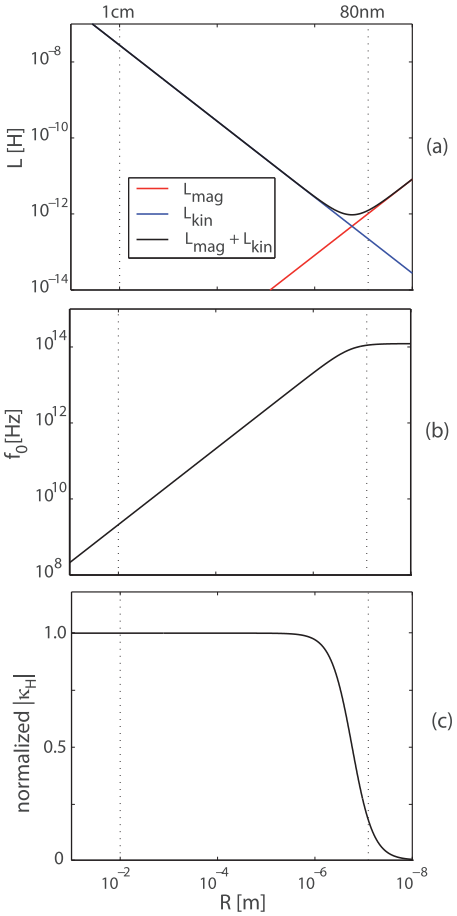

FIG. 8. Scaling down from GHz to THz. (a) Magnetic, kinetic, and total inductance from Eqs. (24) and (26). (b) Resonant frequency from Eq. (27). (c) Magnetic coupling strength from Eq. (29).

Figure 8 aims to illustrate schematically the transition from the GHz to the THz regime. Figure 8(a) shows the effect of the scaling down on the competition between the magnetic inductance and the kinetic inductance, allowing to identify both regimes where either of the contributions to the inductance dominate: $L_{\text{mag}} > L_{\text{kin}}$ (GHz regime) and $L_{\text{mag}} < L_{\text{kin}}$ (THz regime). Figure 8(b) shows the familiar variation of the resonant frequency with element size exhibiting a distinct behaviour in both regimes: linear variation with inverse dimension (GHz regime) and saturation (THz regime). Figure 8(c) shows the magnitude of the magnetic coupling constant, predicting that upon entering the THz regime the magnetic coupling would gradually vanish as the kinetic inductance takes over.

To verify the validity of the approximate Eq. (26), we have determined the kinetic inductance also by the following method. For a given split ring, we found first the resonant frequency from simulations assuming perfect electric conductors, a model that cannot account for kinetic inductance. Next, we assume the permittivity of silver as taken by the Drude model with plasma frequency, $\omega_{\text{p}} = 1.35 \cdot 10^{16}$ rad/s, and collision frequency, $\gamma = 33$ THz, and carry out the simulation again. This, being a realistic model, gives correctly the actual resonant frequency. From the two resonant frequencies, the ratio of kinetic to magnetic inductance can be determined.

In order to find analytically the coupling coefficient, we only need to add the kinetic inductance to the magnetic inductance and we can use the same expression. We performed these calculations for 12 different rings of the same shape ($w = 0.1\ R$, $h = 0.5\ R$, $g = 0.15\ R$) gradually reducing the inner radius R from 10 mm to 80 nm. For the ring with $R = 80$ nm, the resonant frequency is 96.65 THz, close to the saturation frequency of 107 THz. Further scaling down hardly changes the coupling maps; therefore, it is the smallest ring we need to consider. We shall now plot in Figs. 9 and 10 the orientational maps at this frequency, analogous to those plotted in Figs. 3 and 5, respectively. The total coupling coefficient calculated from the analytical model is shown in the top row of Fig. 9, and the one determined from the numerical model in Fig. 10. The agreement is quite good. The magnetic and electric coupling coefficients calculated from the analytical model are shown in the 2nd and 3rd row of Fig. 9, respectively.

For this particular size of the element the kinetic inductance is 4.87 times larger than the magnetic inductance (very close to the analytical value of 4.64 from Eqs. (24) and (26)), the result is a dramatic reduction of the magnitude of the magnetic coupling, namely, by the factor $(L_{\text{mag}} + L_{\text{kin}})/L_{\text{mag}} = 5.87$ (note the different scale used on the color map for magnetic coupling). As a consequence, the total coupling for most

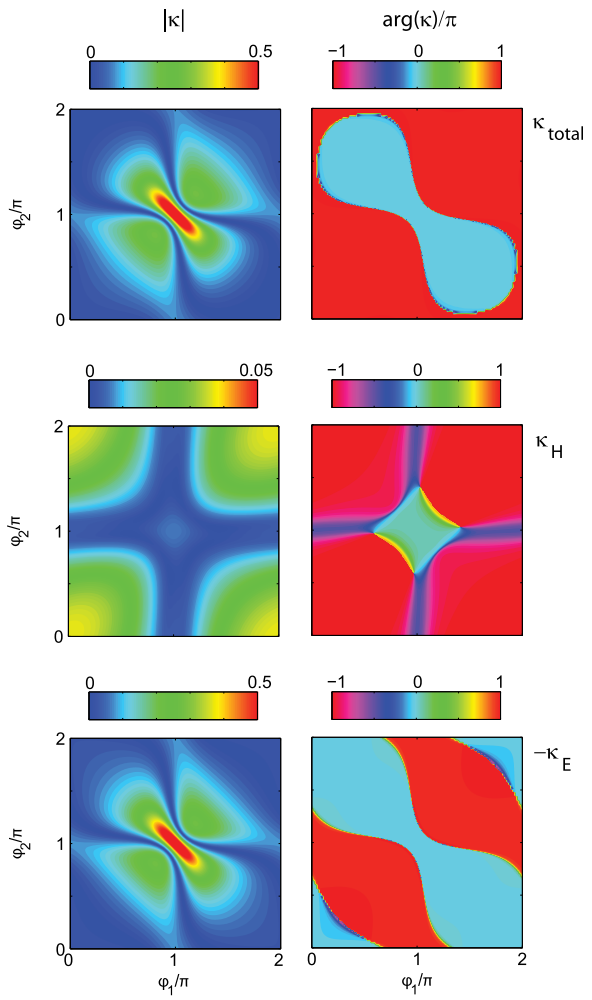

FIG. 9. THz regime. Analytically calculated orientational maps ($R = 80$ nm, $d = 192$ nm, and $f_0 = 96.65$ THz).

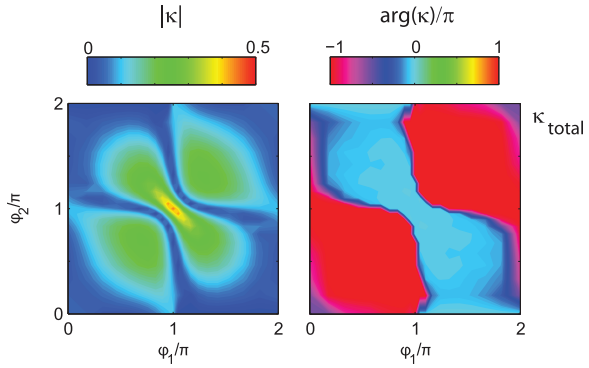

FIG. 10. THz regime. Numerically calculated orientational maps of the total coupling coefficient for the same parameters as in Fig. 9.

configurations is due to the electric contribution only. Another consequence of the saturation of the resonance due to the electron's inertia is a dramatic reduction of the effect of retardation. This is not surprising; after all, the ratio of the mean ring diameter to the wavelength reduces from 0.13 for the GHz split ring to 0.05 for the THz split ring.

The total coupling coefficients obtained from simulation and from the analytical results are compared in Fig. 11. The agreement is good except, as in previous examples, in the

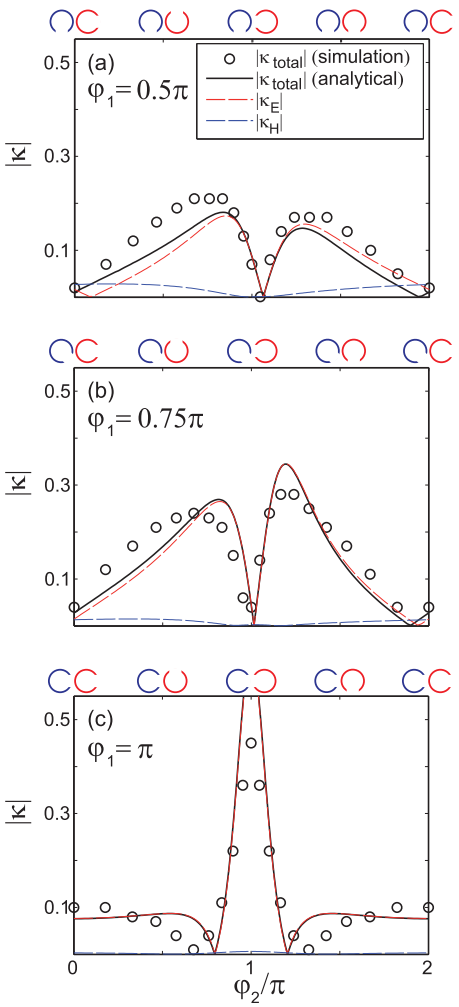

FIG. 11. THz regime ($R = 80$ nm, $d = 192$ nm, and $f_0 = 96.65$ THz). Simulated and analytically calculated coupling coefficients vs. φ_2 for $\varphi_1 = 0.5\pi$ (a), 0.75π (b), and π (c).

"near" configuration. The peak value is actually 0.75, about the same value as obtained in the GHz regime.

IV. CONCLUSIONS

Split-ring resonator is the workhorse of metamaterials research. Hence, it would be greatly beneficial to know all its properties in the whole frequency range up to the saturation of the resonant frequency. We have performed a fundamental piece of research by finding the coupling coefficients between split rings in any position or orientation relative to each other. We have approached the problem from four different directions: two of them analytical relying on circuits and fields (including retardation and kinetic inductance), the third one is simulation, and the fourth one is measurement. The results for co-planar arbitrarily oriented rings have been presented in the form of orientational maps offering both the amplitude and phase of all three coupling coefficients: electric, magnetic, and total. Good quantitative agreement for the total coupling coefficients has been obtained between results acquired by different methods for all configurations except the "near" one where the agreement is only qualitative. It has been shown that depending on orientation, the magnetic and electric couplings may reinforce each other or may act in opposite directions. In the absence of retardation, the coupling coefficients can only be positive or negative, but when retardation is included the coupling coefficient, as may be expected, becomes complex. The retardation effect is shown to be much reduced for the ring investigated in the THz regime near to saturation of the resonant frequency. We have proven that the inertia of electrons, noticeable in the THz regime, is responsible not only for the saturation of the resonant frequency but also for the dramatic reduction of the magnitude of the magnetic coupling, as the geometry is scaled down. Our method is easily adjustable to meta-atoms of arbitrary shape if, instead of relying on analytical approximate expressions for charge and current distribution on a single element, numerical values are used. Our approach will facilitate the design of metamaterials in a wide frequency range up to the saturation of the resonant frequency.

ACKNOWLEDGMENTS

Financial support of the German Research Foundation (DFG), the Russian Foundation for Basic Research (RFFI), and the Leverhulme Trust is gratefully acknowledged.

[1]C. Rockstuhl, C. Menzel, T. Paul, T. Pertsch, and F. Lederer, Phys. Rev. B **78**, 155102 (2008).
[2]C. Tserkezis, N. Papanikolaou, G. Gantzounis, and N. Stefanou, Phys. Rev. B **78**, 165114 (2008).
[3]X. Zhang, M. Davanço, Y. Urzhumov, G. Shvets, and S. R. Forrest, Phys. Rev. Lett. **101**, 267401 (2008).
[4]J. B. Pendry, Phys. Rev. Lett. **85**, 3966 (2000).
[5]J. Pendry, D. Schurig, and D. R. Smith, Science **312**, 1780 (2006).
[6]D. Schurig, J. J. Mock, B. J. Justice, S. A. Cummer, J. B. Pendry, A. F. Starr, and D. R. Smith, Science **314**, 977 (2006).
[7]T. Ergin, N. Stenger, P. Brenner, J. B. Pendry, and M. Wegener, Science **328**, 337 (2010).
[8]N. Liu, H. Liu, S. Zhu, and H. Giessen, Nat. Photonics **3**, 157 (2009).
[9]N. Liu, H. Guo, L. Fu, S. Kaiser, H. Schweizer, and H. Giessen, Nature Mater. **7**, 31 (2008).
[10]C. M. Soukoulis and M. Wegener, Science **330**, 1633 (2010).
[11]O. Sydoruk, E. Tatartschuk, E. Shamonina, and L. Solymar, J. Appl. Phys. **105**, 014903 (2009).
[12]E. Tatartschuk, E. Shamonina, and L. Solymar, Opt. Express **17**, 8447 (2009).
[13]R. R. A. Syms, E. Shamonina, V. Kalinin, and L. Solymar, J. Appl. Phys. **97**, 064909 (2005).
[14]J. D. Baena, L. Jelinek, R. Marques, and M. Silveirinha, Phys. Rev. A **78**, 013842 (2008).
[15]E. Shamonina, V. A. Kalinin, K. H. Ringhofer, and L. Solymar, Electron. Lett. **38**, 371 (2002).
[16]E. Shamonina, V. A. Kalinin, K. H. Ringhofer, and L. Solymar, J. Appl. Phys. **92**, 6252 (2002).
[17]O. Sydoruk, A. Radkovskaya, O. Zhuromskyy, E. Shamonina, M. Shamonin, C. J. Stevens, D. J. Edwards, G. Faulkner, and L. Solymar, Phys. Rev. B **73**, 224406 (2006).
[18]H. Liu, D. A. Genov, D. M. Wu, Y. M. Liu, J. M. Steele, C. Sun, S. N. Zhu, and X. Zhang, Phys. Rev. Lett. **97**, 243902 (2006).
[19]T. Li, R. X. Ye, C. Li, H. Liu, S. M. Wang, J. X. Cao, S. N. Zhu, and X. Zhang, Opt. Express **17**, 11486 (2009).
[20]H. Liu, D. A. Genov, D. M. Wu, Y. M. Liu, Z. W. Liu, C. Sun, S. N. Zhu, and X. Zhang, Phys. Rev. B **76**, 073101 (2007).
[21]G. Dolling, M. Wegener, A. Schädle, S. Burger, and S. Linden, Appl. Phys. Lett. **89**, 231118 (2006).
[22]N. Liu, L. W. Fu, S. Kaiser, H. Schweizer, and H. Giessen, Adv. Mater. **20**, 3859 (2008).
[23]M. Beruete, M. J. Freire, R. Marques, F. Falcone, and J. D. Baena, Appl. Phys. Lett. **88**, 083503 (2006).
[24]M. C. K. Wiltshire, E. Shamonina, I. R. Young, and L. Solymar, Electron. Lett. **39**, 215 (2003).
[25]M. J. Freire and R. Marques, Appl. Phys. Lett. **86**, 182505 (2005).
[26]M. J. Freire and R. Marques, J. Appl. Phys. **100**, 063105 (2006).
[27]O. Sydoruk, M. Shamonin, A. Radkovskaya, O. Zhuromskyy, E. Shamonina, R. Trautner, C. J. Stevens, G. Faulkner, D. J. Edwards, and L. Solymar, J. Appl. Phys. **101**, 073903 (2007).
[28]M. J. Freire and R. Marques, J. Appl. Phys. **103**, 013115 (2008).
[29]L. Solymar, O. Zhuromskyy, O. Sydoruk, E. Shamonina, I. R. Young, and R. R. A. Syms, J. Appl. Phys. **99**, 123908 (2006).
[30]J. K. Gansel, M. Thiel, M. S. Rill, M. Decker, K. Bade, V. Saile, G. von Freymann, S. Linden, and M. Wegener, Science **325**, 1513 (2009).
[31]D. A. Powell, K. Hannam, I. V. Shadrivov, and Y. S. Kivshar, Phys. Rev. B **83**, 235420 (2011).
[32]N. Liu, S. Kaiser, and H. Giessen, Adv. Mater. **20**, 4521–4525 (2008).
[33]L. D. Landau and E. M. Lifschitz, *Electrodynamics of Continuous Media* (Pergamon, Oxford, 1984).
[34]K. Simonyi, *Foundations of Electrical Engineering* (Pergamon, Oxford, 1963).
[35]J. E. Allen and S. E. Segre, Nuovo Cimento **21**, 980 (1961).
[36]V. Delgado, O. Sydoruk, E. Tatartschuk, R. Marques, M. J. Freire, and L. Jelinek, Metamaterials **3**, 57 (2009).
[37]F. Hesmer, E. Tatartschuk, A. Radkovskaya, O. Zhuromskyy, and E. Shamonina, Phys. Status Solidi B **244**, 1170 (2007).
[38]M. Decker, S. Linden, and M. Wegener, Opt. Lett. **34**, 1579 (2009).
[39]M. Decker, S. Burger, S. Linden, and M. Wegener, Phys. Rev. B **80**, 193102 (2009).
[40]In the simulations, an adaptive meshing was used. The grid step varied gradually from 0.17 mm inside the particles to 9 mm in free space. Open boundary conditions were used. Computer Simulation Technology AG (www.cst.com).
[41]S. Linden, C. Enkrich, M. Wegener, J. Zhou, T. Koschny, and C. M. Soukoulis, Science **306**, 1351 (2004).
[42]J. Zhou, T. Koschny, M. Kafesaki, E. N. Economou, J. B. Pendry, and C. M. Soukoulis, Phys. Rev. Lett. **95**, 223902 (2005).
[43]M. W. Klein, C. Enkrich, M. Wegener, C. M. Soukoulis, and S. Linden, Opt. Lett. **31**, 1259 (2006).
[44]S. Tretyakov, Metamaterials **1**, 40 (2007).
[45]L. Solymar, *Lectures on Electromagnetic Theory* (Oxford University Press, Oxford, 1984).
[46]E. A. Coronado and G. C. Schatz, J. Chem. Phys. **119**, 3926 (2003).
[47]V. P. Drachev, U. K. Chettiar, A. V. Kildishev, H.-K. Yuan, W. Cai, and V. M. Shalaev, Opt. Express **16**, 1186 (2008).